Centering of a radial microtubule array by translocation along microtubules spontaneously nucleated in the cytoplasm

Viacheslav Malikov[1], Eric N. Cytrynbaum[2], Anna Kashina[3], Alexander Mogilner[4] and Vladimir Rodionov[1,5]

Positioning of a radial array of microtubules (MTs) in the cell centre is crucial for cytoplasmic organization, but the mechanisms of such centering are difficult to study in intact cells that have pre-formed radial arrays. Here, we use cytoplasmic fragments of melanophores, and cytoplasts of BS-C-1 cells to study MT centering mechanisms. Using live imaging and computer modelling, we show that the MT aster finds a central location in the cytoplasm by moving along spontaneously nucleated non-astral MTs towards a point at which MT nucleation events occur equally on all sides. We hypothesize that similar mechanisms, in the presence of the centrosome, contribute to this centering mechanism and ensure the robustness of cytoplasmic organization.

The radial array of cytoplasmic microtubules (MTs) determines the spatial organization of the cytoplasm. The central position of an MT aster is actively maintained in living cells, but the nature of the centering mechanisms is poorly understood. Recent work[1] indicates that dynein motors have an important role, as they are bound to the cell cortex, which pulls on centrosomal MTs. Other forces, including actomyosin contractility and MT polymerization pushing against the cortex, can also contribute to the centering process[1].

Studies of the centering mechanisms that occur in intact cells are possible but there are restrictions: the centrosome is pre-positioned in the cell centre and such studies would require displacing it from the centre in the first place — a task that, in itself, affects the organization of the cytoplasm and MTs. Thus, it seems necessary to find a suitable model system, which is similar to a living cell in every aspect, has no pre-centered radial array of MTs, and rapidly forms such an array in an observable manner. We have recently developed such a system by using microsurgically produced cytoplasmic fragments of fish melanophores — pigment cells, the function of which is aggregation of pigment granules in the cell centre or re-dispersion throughout the cytoplasm by

means of MT motors of the dynein (aggregation) or kinesin (dispersion) families[2]. In such fragments, MTs are randomly oriented and can be induced to form a centrally positioned MT aster that is similar to that in the intact cell[3,4]. This occurs by application of pigment aggregation stimuli that cause pigment granules — primary sites for MT nucleation in the absence of the centrosome[4,5] — to form an aggregate that becomes the focal point of the aster. If melanophores are stimulated to aggregate pigment granules immediately after dissection, the pigment aggregate in such nascent fragments initially forms at the proximal (cut) edge of a fragment and then relocates to the centre.

Fig. 1a and Supplementary Information, Movie 1 illustrate the kinetics of the centering of a pigment aggregate in the nascent melanophore fragment. This kinetics is described with a single exponential curve, $t_{1/2} \sim 10$ min. In intact cells, centering of a radial MT array relies on pulling and/or pushing forces that are produced by growing MT ends (MT dynamics), cortical dynein motors and actomyosin contractility[1]. Our past work has shown that inhibition of MT dynamics by an MT-stabilizing drug, taxol, results in the inability of an MT array to centre in a nascent melanophore fragment[3]. To find out whether the activity of cytoplasmic dynein and actomyosin contractility are also required for centering, we injected the dynein inhibitor sodium orthovanadate into nascent fragments after the formation of a pigment aggregate at the margin of the nascent fragment[6]. We also treated nascent fragments with an actin inhibitor, latrunculin B, at a concentration ($5\,\mu M$) that completely depolymerizes actin filaments in melanophores and inhibits actin-dependent transport of pigment granules[7]. Following injection of vanadate (a needle concentration of $10\,\mu M$), the centripetal movement of the pigment aggregate was completely inhibited (Fig. 1b, 1d), but latrunculin B treatment did not affect the movement kinetics (data not shown). We conclude that the centering mechanism in melanophore fragments does not involve the actin cytoskeleton but requires the activity of cytoplasmic dynein motors and MT dynamics. Control experiments demonstrated that neither injection of vanadate nor latrunculin
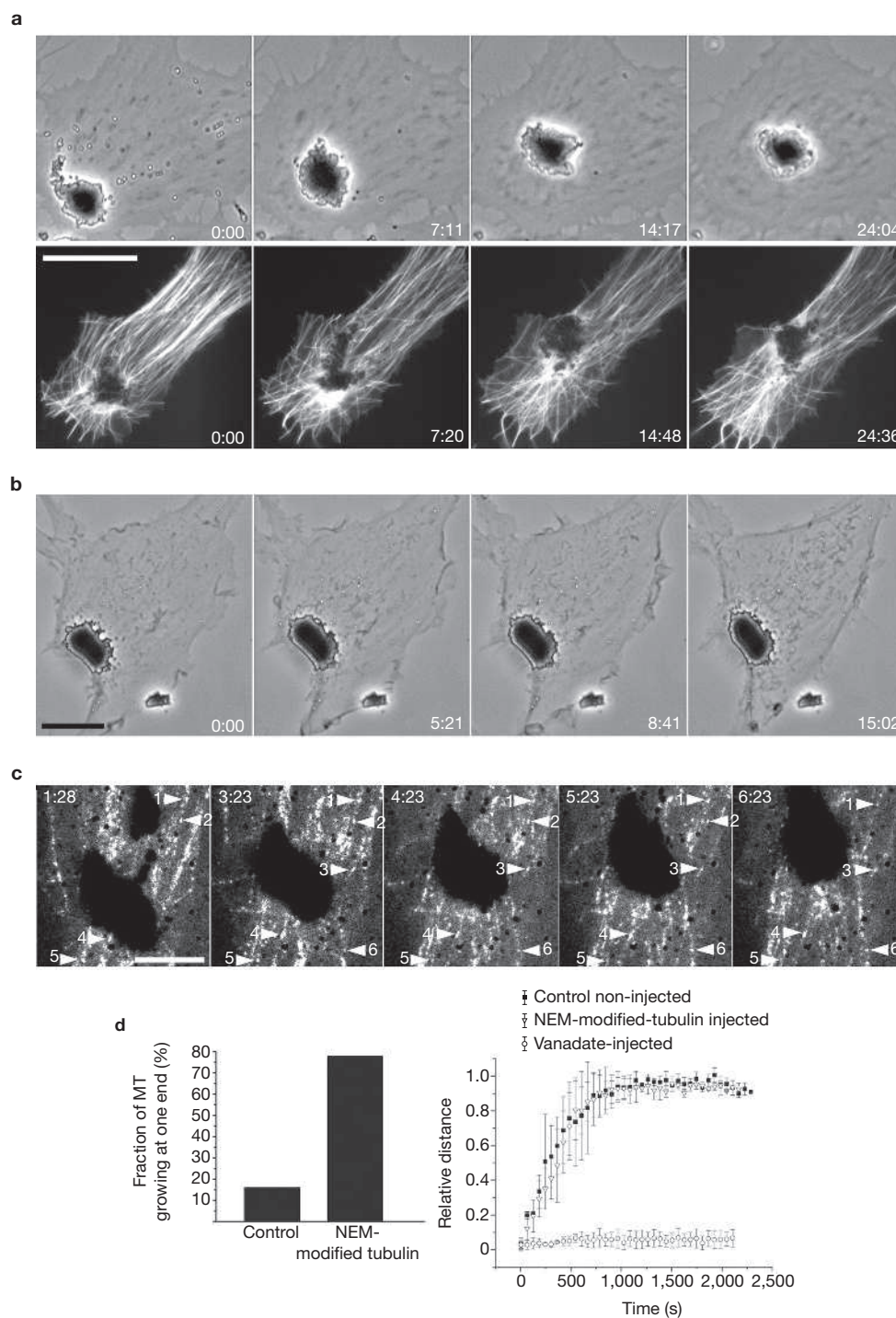
Figure 1 Centering of the MT array in melanophore fragments is driven by cytoplasmic dynein. Centripetal movement of the pigment aggregate in nascent fragments of melanophores depends on the activity of cytoplasmic dynein and does not involve minus-end microtubule (MT) growth or the movement of MTs in the cytoplasm. (**a**) Time sequences of control non-injected fragments; phase-contrast images (top panel) and fluorescence images of MTs (bottom panel). (**b**) Time sequence of phase-contrast images of a fragment injected with sodium orthovanadate (at a needle concentration of 10 μM) after aggregation of pigment granules at the cut edge. (**c**) Time sequence of fluorescence images of speckles on MTs produced by injecting the parent cell with tubulin given at a low (0.5 mg ml⁻¹) concentration. (**d**) Centripetal movement of the pigment aggregate in the fragments injected with inhibitor of minus-end MT growth, NEM-modified tubulin. Left panel, fraction of MT seeds that elongated at only one end in the absence (left bar) or in the presence (right bar) of NEM-modified tubulin *in vitro*; a small fraction of NEM-modified tubulin subunits (<10%) induces a ~5-fold increase in the fraction of seeds that grew at only one (presumably, plus) end, indicating a high inhibitory effect on minus-end growth. Right panel, kinetics of changes in relative distance between the centre of the aggregate and the cut edge in control non-injected fragments (filled squares) and in the fragments injected with NEM-modified tubulin (at a needle concentration of 20 mg ml⁻¹); the curve obtained for sodium orthovanadate-injected fragments (needle concentration 10 μM) is shown for comparison (open circles). Numbers on panels **a**–**c** indicate time in min. Scale bars, 10 μm (**a**, **b**) and 5 μm (**c**).
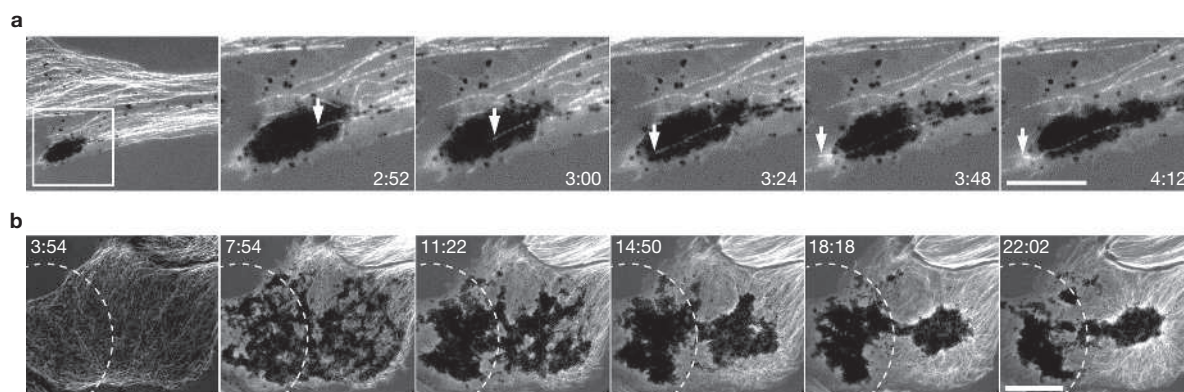
Figure 2 Centering of the pigment aggregate involves targeting by the microtubules that spontaneously nucleate in the cytoplasm. (**a**) Time sequence of live images of microtubules (MTs) and pigment granules in a nascent fragment. Main image in left panel, is a low-magnification image. Other images are successive high-magnification images of MTs and pigment granules in the boxed region shown in the left panel; arrows mark positions of the growing (plus) end of a MT that nucleated on the distal side and served as a pathway for transport of the pigment granules to the centre. (**b**) Time sequence of live images of MTs and pigment granules in a fragment that was locally treated with nocodazole solution applied through a micropipette in the area depicted with a dashed line. Numbers indicate time in min. Scale bars, 5 µm (**a**) and 20 µm (**b**).

B treatment significantly affected the rates of growth or shortening of MTs in the fragments (data not shown).

MT-dependent centering mechanisms in intact cells involve movements of the MT array in the cytoplasm[1]. However, the results of our past work using photobleaching argue against an MT-transport-based centering mechanism in the fragments[3]. A possibility remains, however, that centering of the pigment aggregate is driven by the movement of a small fraction of MTs, which previously escaped detection due to the low spatial resolution of the photobleaching experiments. We therefore reinvestigated the possibility of MT movement by using fluorescent speckle microscopy, an approach that involves the generation of fiduciary marks (speckles) along the length of individual MTs[8] and, therefore, allows high-resolution detection of their movement in the cytoplasm. Rigorous analysis of several dozens of fragments containing hundreds of MTs showed that speckles always remained immotile and so redistribution of pigment aggregate to the centre occurred along the framework of stationary MTs (Fig. 1c; and see Supplementary Information, Movie 2). We therefore conclude that centering in the nascent fragment, unlike in intact cells, does not involve the movement of the entire MT array by application of pulling or pushing forces on MTs.

As dynein activity and MT dynamics are required for centering in the fragment, but MT movements during centering do not occur, we next assessed whether centering could be driven by dynein-dependent MT growth at the minus ends — a mechanism that has been suggested but never observed in living cells before. To test this possibility, we injected nascent fragments after the formation of the pigment aggregate at the margin with an inhibitor of minus-end MT assembly (NEM-modified tubulin), which was prepared according to a published experimental protocol[9] and pre-tested *in vitro* to inhibit MT growth at the minus ends with high efficiency (Fig. 1d, left). Injection of NEM-modified tubulin at a needle concentration of 20 mg ml^{-1} — which is estimated to be equal to ~10% of the total intracellular tubulin or 2 mg ml^{-1} intracellular concentration, an amount that is sufficient to inhibit MT minus-end polymerization *in vitro* by 90% — had no effect on the pigment aggregate movement kinetics (Fig. 1d, right). We therefore conclude that centering of the pigment aggregate in the fragments does not involve MT polymerization at the minus ends.

As centering in the fragment occurs in a dynein-dependent manner along stationary MTs and does not involve nucleation at the minus ends or pulling at the actomyosin cortex, it seems that the behaviour of MTs themselves is involved in the centering mechanisms. To analyse, in detail, the behaviour of MTs during centering, we examined the time-series of high-resolution images of MTs and pigment granules in nascent fragments during the movement of the pigment aggregate from the fragment edge to the centre. This analysis showed that movement of the pigment aggregate seems to be driven by transport of pigment granules along MTs away from the cut edge. This transport was facilitated by MTs that nucleated in the cytoplasm and grew towards the pigment aggregate, therefore seeming to be of opposite polarity to the dominant astral MTs ('anti-astral' polarity). Often, contact of a single MT with the pigment aggregate was sufficient for significant displacement of the aggregate towards the centre (Fig. 2a; and see Supplementary Information, Movie 3). These centripetal displacements continued until the MTs with 'anti-astral' polarity depolymerized from their minus ends (data not shown).

These observations indicate that pigment granules are continuously transported along newly nucleated MTs and there is no apparent preference for some MTs over others. As these granules eventually end up in the centre of the aggregate, there must be a mechanism that ensures that their preferential displacement would occur towards the centre of the fragment. We hypothesized that such preferential displacement could be controlled by an asymmetry in the amount of MT nucleation sites on different sides of the aggregate. To test this hypothesis, we introduced asymmetry into the MT array during centering by treating them locally with the MT drug nocodazole, which was applied through a micropipette (at a needle concentration of 10 µM). Such treatment results in local disassembly of MTs and prevents their nucleation and growth in an area of the cytoplasm that is proximal to the micropipette[1], which therefore loses the ability to supply MTs that are capable of supporting pigment transport. If centering of the pigment aggregate occurs through the asymmetric nucleation of MTs, MT asymmetry in nocodazole-treated fragments should induce displacement of the aggregate away from the treated zone towards a final location in the centre of the intact area of the cytoplasm and not in the geometrical centre of the fragment. In agreement with the published results[1], the number of MTs in the area of the cytoplasm in the vicinity
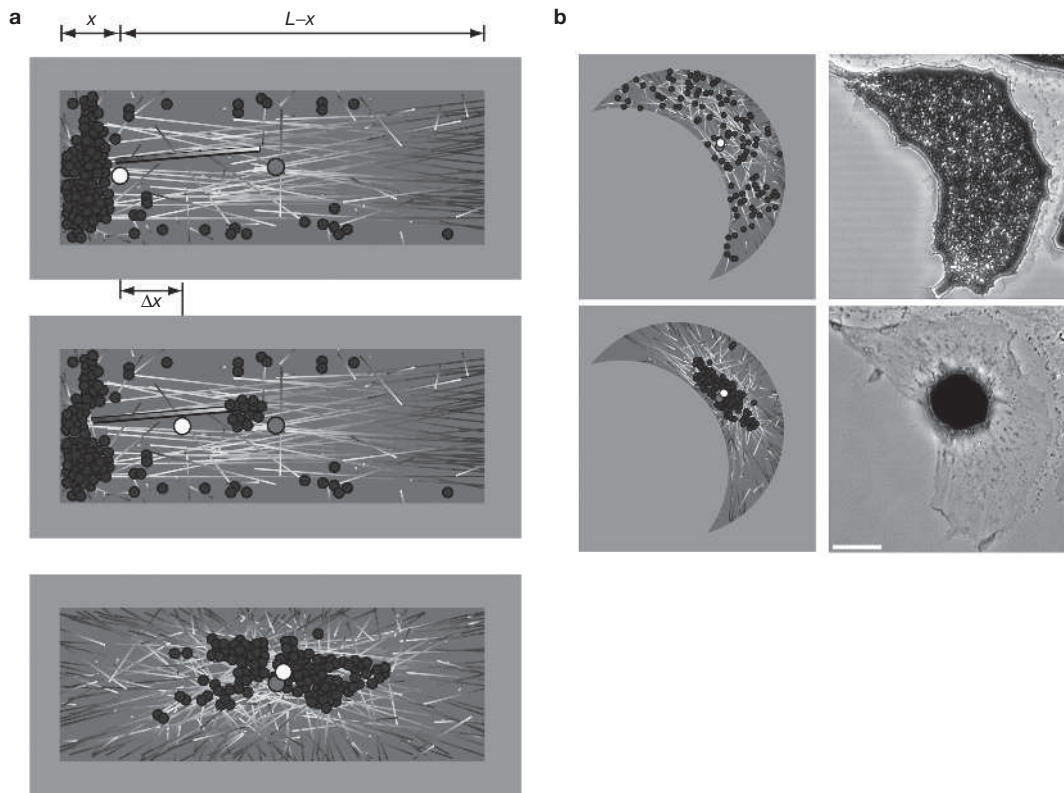
Figure 3 Computational simulation of centering of the pigment aggregate.
(**a**) Snapshots from the simulation of centering of the pigment aggregate in a rectangular, elongated fragment. Top panel, initially microtubules (MTs) are oriented with their minus (light) and plus (dark) ends at the left and right, respectively. Middle panel, a single self-nucleated MT (dark, middle panel) can translocate a significant number of granules towards the centre. Bottom panel, in a few tens of minutes, the granules aggregate near the centre of the fragment, whereas MTs self-organize into the aster with the aggregate at the focal point; circles indicate positions of the centroids of the pigment aggregate (white) and the fragment (grey). x and $(L-x)$ are the initial distances of the granule centre-of-mass from the left and right edges of the fragment, respectively. Δx is the shift of the granule centre-of-mass towards the centre of the fragment due to transport of a number of granules to the minus end of a single self-nucleated MT. (**b**) Centering of the pigment aggregate in crescent-shaped fragments. Left panel, snapshots from computational simulation; circles indicate positions of the centroids of the pigment aggregate (white) and the fragment (grey). Right panel, phase-contrast images of a fragment before (top) and 20 min after (bottom) stimulation of pigment aggregation with adrenalin. Scale bar, 10 μm.

of the micropipette (Fig. 2b, dashed line) was significantly reduced after 20 min of nocodazole treatment. Stimulation of such nocodazole-treated fragments with adrenalin resulted in slow clumping of pigment granules in the nocodazole-treated area, which is probably explained by pigment transport along the sparse residual MTs. By contrast, in the nocodazole-free area, MTs rapidly organized into a radial array and pigment granules aggregated at the focal point of converging MTs. Remarkably, the position of the pigment aggregate corresponded to the centre of the area of the cytoplasm that contained intact MTs, and not to the geometric centre of the fragment (Fig. 2b). Therefore, the area of the cytoplasm with active MT growth and nucleation determines the direction of the displacement of the aggregate, supporting the hypothesis that local nucleation of MTs provides the mechanism for the aggregate movement and centering.

To confirm that the proposed mechanism can drive the centering of the radial array in the absence of other centering mechanisms, we developed a two-dimensional computational model that simulates the centering kinetics in a melanophore fragment (Fig. 3; and see Supplementary Information, Methods, Movies 4 and 5, and Figs S1–S4). The model translates known and plausible assumed properties of the MT and granule dynamics into mathematical terms and uses stochastic computer simulations to reconstitute the MT-granule system *in silico*. In close agreement with experimental results, the centering kinetics and the final position

of the pigment aggregate in the fragments of different shapes closely corresponded to the experimental data (Fig. 3b; and see Supplementary Information, Movie 5 and Fig. S3). The model tested the importance of the dynamic properties of the MTs that are impossible to investigate experimentally and predicted that: plus-end MT growth rate is an important parameter that determines the centering time scale; and that changes in global rates of MT nucleation do not significantly affect the centering rate. However, the ratio of MTs that are nucleated locally on the pigment granules to those nucleated at the random sites in the cytoplasm is of crucial importance and has to be between 0.1 and 0.25 to enable an optimum centering rate. These and other predictions and their biological implications are discussed in Supplementary Information, Methods.

To test whether the same centering mechanisms work in non-pigment cells, we produced enucleated cytoplasts of BS-C-1 cells and observed spontaneous formation of a MT radial array by incubation in culture. To produce such cytoplasts, we treated BS-C-1 cells with a combination of actin-depolymerizing latrunculin B and MT-depolymerizing nocodazole, followed by upside-down centrifugation at low speeds[10]. It has been found that such a procedure results in the formation of equal amounts of centrosome-free and centrosome-containing cytoplasts with depolymerized MTs, allowing simultaneous observation of MT radial-array formation and centering with and without a centrosome.
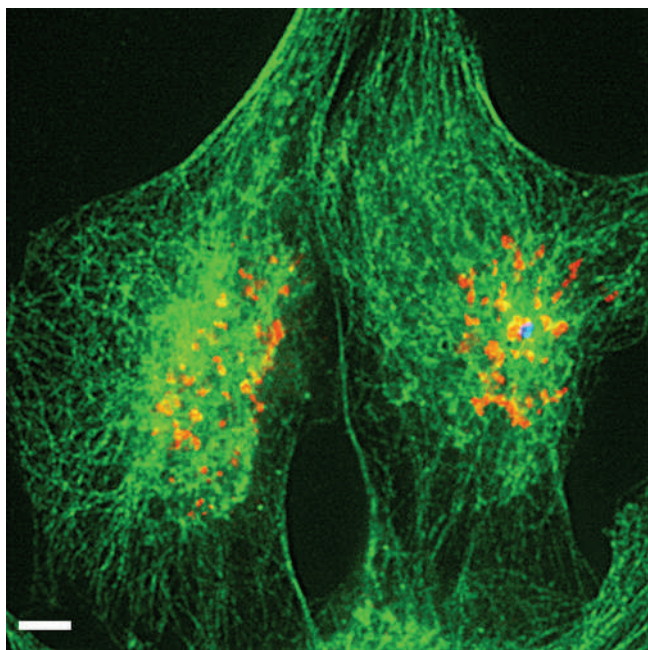
Figure 4 Microtubules in cytoplasts of BS-C-1 cells attain radial organization. Cytoplasts of BS-C-1 cells were prepared using centrifugation in the presence of nocodazole and latrunculin B[13] and triple-immunostained with antibodies against pericentrin (blue), tubulin (green) and a Golgi protein with a relative molecular mass of 58,000 (red) to reveal the centrosome and the distribution of microtubules (MTs) and Golgi membranes, respectively. Similar to the centrosome-containing cytoplast (right), MTs attained a radial organization and Golgi membranes became positioned in the centre in the centrosome-free cytoplast (left). Scale bar, 10 μm.

Due to the absence of stimuli that could allow us to induce MT centering in the BS-C-1 cytoplasts in a similar way to that in melanophore fragments, we were unable to make live observations of MT centering in the BS-C-1 cytoplasts. Instead, we incubated the nascent BS-C-1 cytoplasts in culture for 12 h, followed by triple antibody staining to visualize MTs, the centrosome and the Golgi complex (Fig. 4). The results of this staining indicated that radial MT arrays were able to form and centre in the cytoplasts regardless of the presence of centrosomes. Moreover, the components of the Golgi complex were found in close proximity to the MT focus in the centre of the cytoplasts, indicating that the centering of these organelles is closely correlated with the centering of the radial array. Whereas this experiment does not prove that the centering in the BS-C-1 cytoplasts occurs in exactly the same way as in melanophore fragments, the resulting MT arrays are inherently similar, as they both emanate from the focus of membranous organelles with dynein and MT nucleation sites on their surface[11,12] and are formed in the absence of the centrosome. Therefore, we believe that the novel centering mechanism described here exists in multiple cell types.

Our results describe a novel mechanism of centering of a radial MT array *in vivo*. This mechanism involves transport of MT nucleation sites along MTs that are spontaneously nucleated and 'treadmilling' in the cytoplasm. Figure 5 shows a schematic representation of the centering of a radial MT array in melanophore fragments. Stimulation of nascent fragments for pigment aggregation activates dynein motors that are bound to pigment granules and initially induces their rapid transport to the cut edge along the preexisting MTs. However, as these MTs are no longer connected to the centrosome, they depolymerize from the minus ends, thereby giving way to the formation of a radial array and
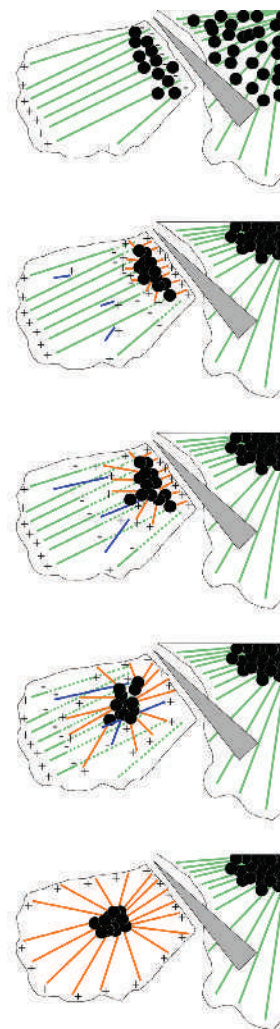

Figure 5 Centering of the pigment aggregate in cytoplasmic fragments of melanophores. Solid green lines, preexisting microtubules (MTs) inherited by a fragment from parent cell. These MTs eventually depolymerize from minus ends (dashed green lines). Red and blue lines, newly assembled MTs form in a fragment via nucleation on pigment granules (red lines) or spontaneously in the cytoplasm (blue lines).

increasing the size of the soluble pool of tubulin subunits that are available for MT assembly. Numerous MTs that are nucleated *de novo* treadmill through the cytoplasm. Once these MTs contact the pigment aggregate, they provide tracks for the movement of pigment granules away from the cut edge. Acting repeatedly, these cycles of MT nucleation, treadmilling and transport of pigment granules lead to the overall movement of the pigment aggregate towards the centre. In the centre, the movement ceases because approximately equal amounts of MTs are nucleated in the cytoplasm surrounding the pigment aggregate.

The two key components that are involved in this centering — MT dynamic behaviour and dynein-dependent transport — are the same as the ones that drive the centering of the centrosomal MT array. However, their roles in the non-centrosomal centering mechanism described here are different. In the centrosomal mechanism, MTs grow from the centrosome and are positioned by the dynein pulling force at the cell cortex[13]. In the newly discovered non-centrosomal mechanism, MTs nucleate spontaneously in the cytoplasm and then serve as rails for dynein-dependent transport of the nucleation sites. Both types of centering occur as a result

of the intrinsic properties of MTs and dynein; however, the newly discovered non-centrosomal centering mechanism describes a previously unknown role for both of these components *in vivo*.

Spontaneous nucleation of MTs is a rare but not unusual event, which has been observed in intact cells[14] and in cytoplasmic fragments[15] and cytoplasts[16] that lack a centrosome. As the MT nucleation rate per unit of cytoplasmic area is probably constant across the cytoplasm, more MTs initially nucleate on the side of the aggregate that is distal to the cut edge. These MTs provide pathways for the transport of pigment granules and direct their movement away from the cut edge. When the aggregate reaches the centre of the fragment, the cytoplasmic area and, therefore, the probability of MT nucleation on all sides of the aggregate becomes equal. This keeps the aggregate in the centre, equidistant from the cell margins.

Our finding that centering occurs similarly in centrosome-free and centrosome-containing cytoplasts indicates that the non-centrosomal centering mechanism exists in all cells regardless of the presence of the centrosome, and possibly contributes to the centering of a radial array in interphase cells. Indeed, the global centering of an astral MT array, which is shown to occur due to the dynein pulling on the relatively long astral MTs at the cell cortex[1], would be much more robust if another mechanism existed in the cell centre to correct the positioning of the centrosome in the exact centre of the cell. Such a mechanism would be difficult to observe in intact cells due to the large amount of material that is found in the vicinity of the centrosome; however, our numerical approximation (see Supplementary Information, Methods) indicates that the probability of the centrosome positioning in the exact centre of the cell (and not in its approximate vicinity) increases significantly (up to 10–20% depending on the model assumptions) in the presence of an additional non-centrosomal centering force. It would be interesting to find out whether MTs of 'anti-astral' polarity exist in close proximity to the centrosome and to determine the exact contribution of the non-centrosomal mechanism to the centering of a centrosomal radial array. □

METHODS

Cell culture. Cultures of black tetra melanophores were prepared as described previously[17]. Aggregation of pigment granules in intact cells and cell fragments was induced with 10^{-5} adrenalin.

Preparation of derivatized tubulin. Porcine brain tubulin depleted of MT-associated proteins was labelled with Cy3-reactive dye (Amersham Biosciences, Piscataway, NJ) as described previously[10] and used at a needle concentration of 8–10 mg ml^{-1}. For fluorescence speckle microscopy[8], a needle concentration of tubulin was reduced to 0.3–0.5 mg ml^{-1}.

NEM-modified tubulin was prepared as described previously[9] and used in microinjection experiments at a needle concentration of 20 mg ml^{-1}. Elongation of fluorescent MT seeds was assayed as described previously[5].

Microinjection and micromanipulation. Microinjection was performed as described previously[10]. Following this injection of fluorescently tagged tubulin cells were incubated for at least 1 h at 30°C to allow for incorporation of labelled tubulin into MTs.

To prepare fragments, melanophore processes were dissected with microneedles with a 0.1 μm-tip diameter[3].

Local disruption of MTs with nocodazole was performed as described in detail previously[1]. Briefly, nocodazole (10 μg ml^{-1}) was applied through a micropipette that was placed at the fragment margin at an angle to the substrate to produce a flow that was directed away from the fragment. To continuously monitor the flow of solution from the micropipette and to visualize the gradient of nocodazole concentration, the nocodazole solution was supplemented with fluorescein at a low (1 μg ml^{-1}) concentration. Focal application of nocodazole rapidly depolymerizes MTs in the proximity to the micropipette but does not affect the dynamics of distal MTs for at least 20 min of treatment[1].

Preparation of cytoplasts of BS-C-1 cells. Cytoplasts of BS-C-1 cells were obtained by cell centrifugation in the presence of nocodazole and latrunculin B as described in detail previously[10], washed three times with fresh tissue culture medium (DMEM/F10 containing 10% fetal bovine serum and antibiotics) and incubated overnight. For localization in the cytoplasts of MTs, the Golgi complex and the centrosome, cytoplasts were fixed with cold methanol and triple stained with sheep tubulin antibody (Cytoskeleton Inc., Denver, CO), rabbit antibody against pericentrin and mouse monoclonal antibody against a Golgi protein with a relative molecular mass of 58,000 (both from Abcam, Cambridge, MA). Secondary antibodies were affinity-purified antibodies that were generated in donkeys against mouse, sheep and rabbit immunoglobulin-G-conjugated-FITC, -TRITC and -Cy5, respectively (Jackson Immunoresearch, West Grove, PA).

Image acquisition and analysis. Fragments dissected from Cy3-injected cells were treated with the oxygen scavenger Oxyrase (Oxyrase Company, Mansfield, OH) to reduce photodamage and photobleaching, as described previously[4]. Images of MTs in the fragments were collected using a Nikon Diaphot 300 microscope equipped with a slow-scan back-illuminated cooled charged-coupled device camera (CH350; Photometrics, Tucson, AZ) that was driven by Metamorph imaging software (Universal Imaging Corp., Downington, PA).

Note: Supplementary Information is available on the Nature Cell Biology website.

1. Burakov, A., Nadezhdina, E., Slepchenko, B. & Rodionov, V. Centrosome positioning in interphase cells. *J. Cell Biol.* **162**, 963–969 (2003).
2. Nascimento, A. A., Roland, J. T. & Gelfand, V. I. Pigment cells: a model for the study of organelle transport. *Annu. Rev. Cell Dev. Biol.* **19**, 469–491 (2003).
3. Rodionov, V. I. & Borisy, G. G. Self-centring activity of cytoplasm. *Nature* **386**, 170–173 (1997).
4. Vorobjev, I., Malikov, V. & Rodionov, V. Self-organization of a radial microtubule array by dynein-dependent nucleation of microtubules. *Proc. Natl Acad. Sci. USA* **98**, 10160–10165 (2001).
5. Malikov, V., Kashina, A. & Rodionov, V. Cytoplasmic dynein nucleates microtubules to organize them into radial arrays *in vivo. Mol. Biol. Cell* **15**, 2742–2749 (2004).
6. Paschal, B. M. & Vallee, R. B. Retrograde transport by the microtubule-associated protein MAP 1C. *Nature* **330**, 181–183 (1987).
7. Rodionov, V. I., Hope, A. J., Svitkina, T. M. & Borisy, G. G. Functional coordination of microtubule-based and actin-based motility in melanophores. *Curr. Biol.* **8**, 165–168 (1998).
8. Waterman-Storer, C. M., Desai, A., Bulinski, J. C. & Salmon, E. D. Fluorescent speckle microscopy, a method to visualize the dynamics of protein assemblies in living cells. *Curr. Biol.* **8**, 1227–1230 (1998).
9. Hyman, A. *et al.* Preparation of modified tubulins. *Methods Enzymol.* **196**, 478–485 (1991).
10. Rodionov, V., Nadezhdina, E., Peloquin, J. & Borisy, G. Digital fluorescence microscopy of cell cytoplasts with and without the centrosome. *Methods Cell Biol.* **67**, 43–51 (2001).
11. Rios, R. M., Sanchis, A., Tassin, A. M., Fedriani, C. & Bornens, M. GMAP-210 recruits γ-tubulin complexes to *cis*-Golgi membranes and is required for Golgi ribbon formation. *Cell* **118**, 323–335 (2004).
12. Allan, V. J., Thompson, H. M. & McNiven, M. A. Motoring around the Golgi. *Nature Cell Biol.* **4**, E236–E242 (2002).
13. Vallee, R. B. & Stehman, S. A. How dynein helps the cell find its center: a servomechanical model. *Trends Cell Biol.* **15**, 288–294 (2005).
14. Yvon, A. M. & Wadsworth, P. Non-centrosomal microtubule formation and measurement of minus end microtubule dynamics in A498 cells. *J. Cell Sci.* **110**, 2391–2401 (1997).
15. Rodionov, V. I. & Borisy, G. G. Microtubule treadmilling *in vivo. Science* **275**, 215–218 (1997).
16. Rodionov, V., Nadezhdina, E. & Borisy, G. Centrosomal control of microtubule dynamics. *Proc. Natl Acad. Sci. USA* **96**, 115–120 (1999).
17. Rodionov, V. I., Lim, S. S., Gelfand, V. I. & Borisy, G. G. Microtubule dynamics in fish melanophores. *J. Cell Biol.* **126**, 1455–1464 (1994).

ERRATUM

Owing to a technical error, the pages of this manuscript were originally mis-numbered by a 100 pages. This has now been corrected online. The corrected online manuscript is numbered 100 pages higher than the mis-numbered version.
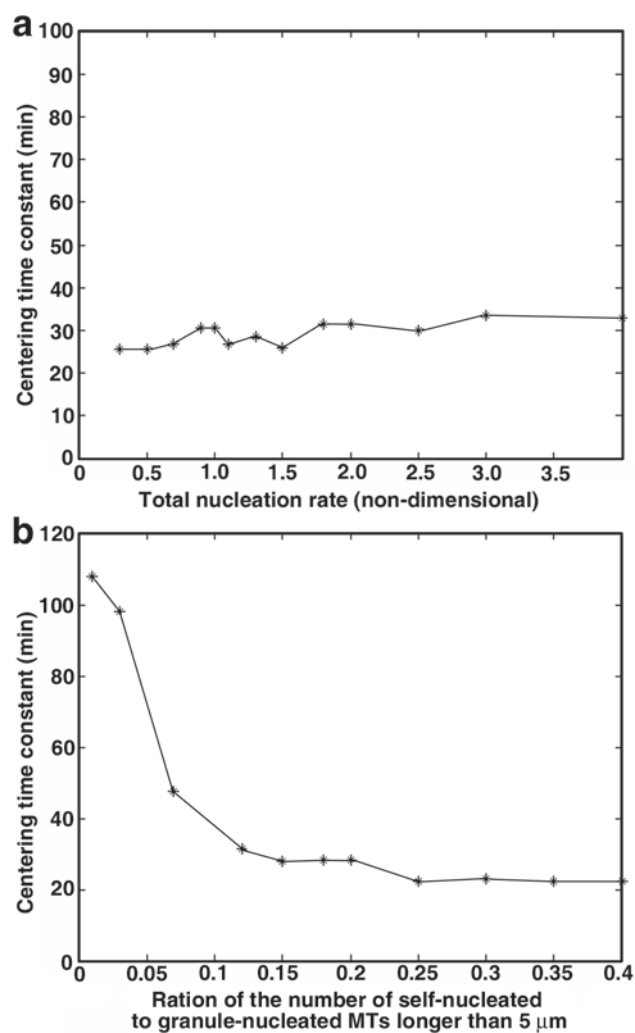
Figure S1 The average centering time is insensitive to the total nucleation rate (a), but is a decreasing function of the ratio of the number of long (longer than 5 μm) self-nucleated MTs to the number nucleated on the pigment granules (b).
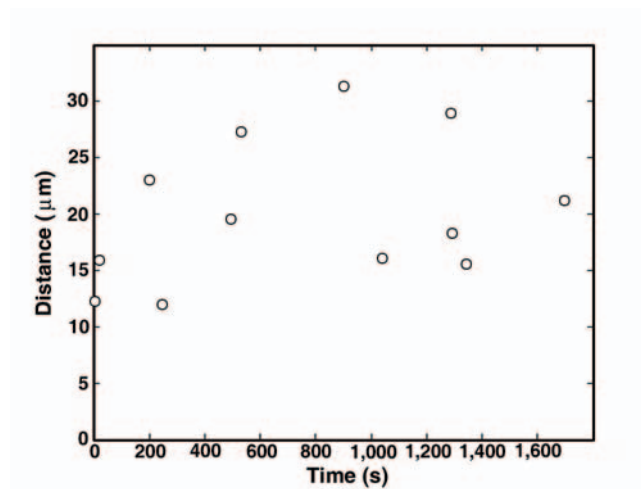
Figure S2 Centering time as a function of the distance traveled by the pigment aggregate's centroid measured in 12 fragments of different length and similar width. Correlation analysis shows a low degree of correlation between the centering time and the fragment size.
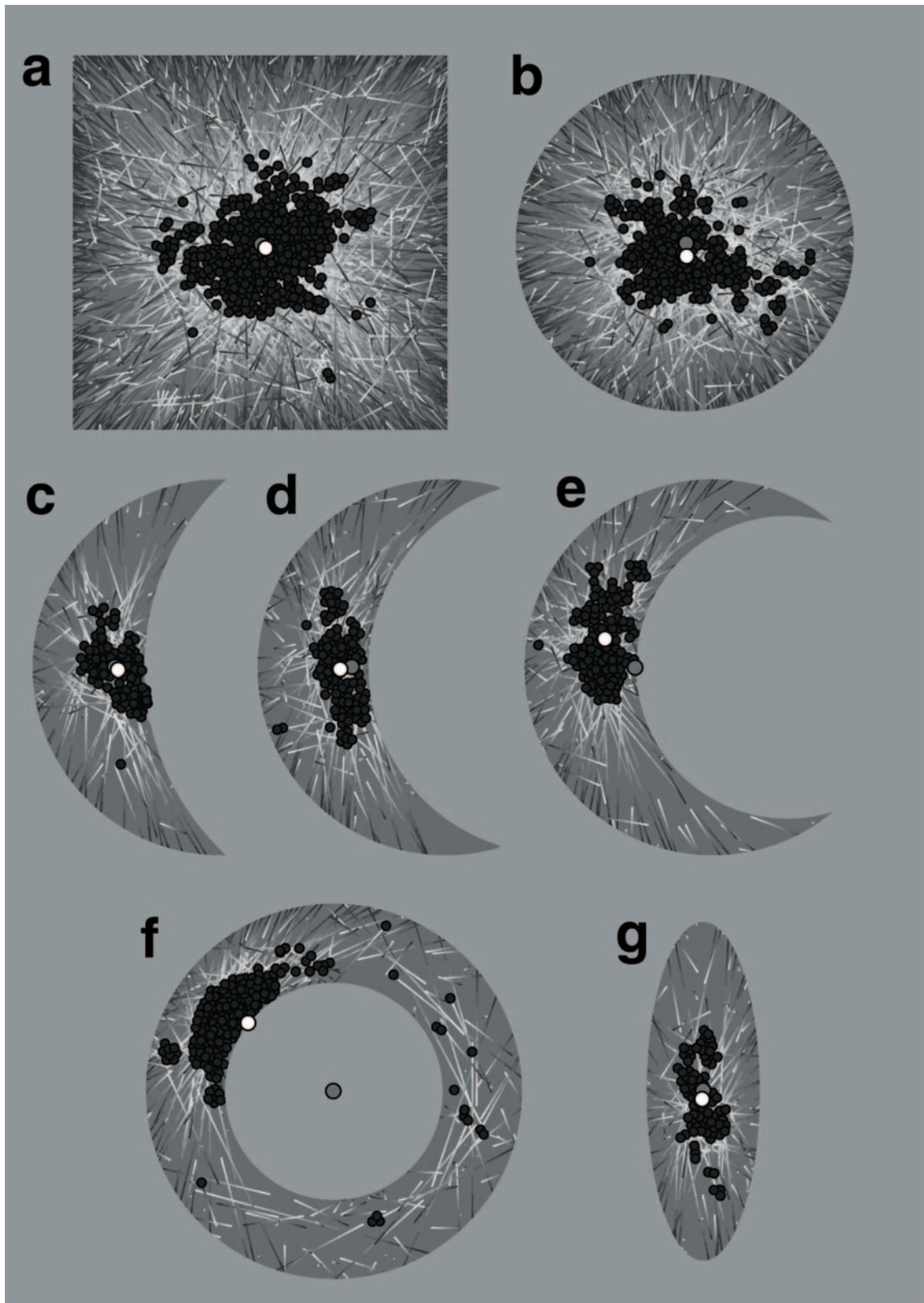
Figure S3 Model simulations predict aggregation of the pigment's centroid (white circle) to the centroid of the fragment (grey circle) in fragments of square (a), circular (b), crescent (c-e) and ellipsoidal (g) shapes. In the toroidal fragment (f), the granules aggregate into a cluster near the inner boundary of the fragment. MTs are plotted with their minus ends light and plus ends dark.
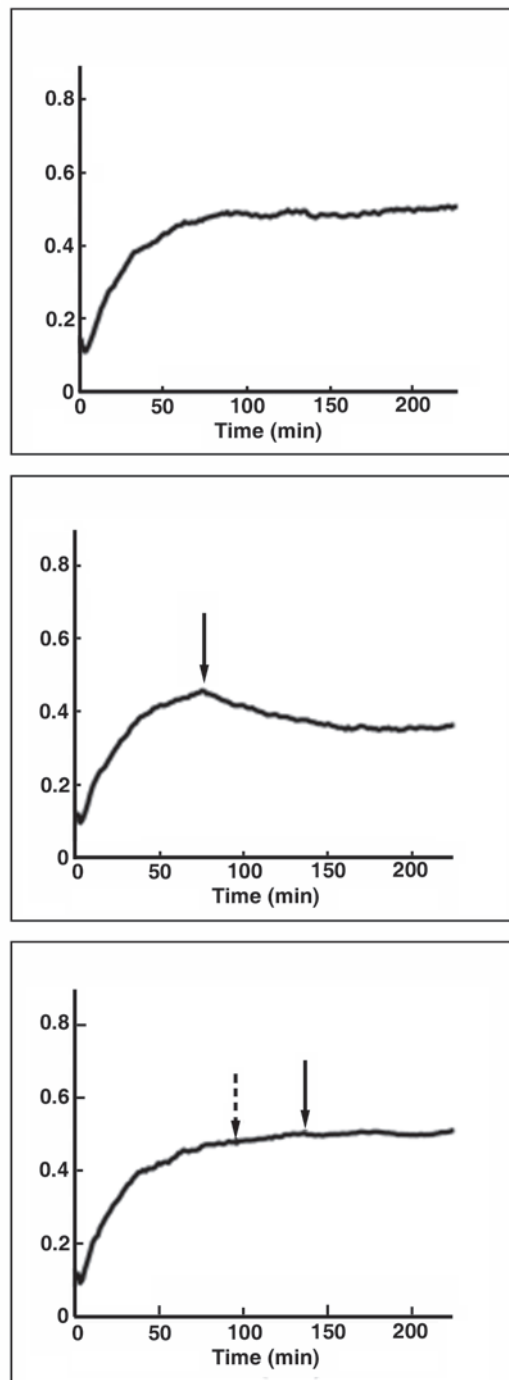
Relative position of pigment centroid

Figure S4 Averaged (n=50) computed position of the pigment aggregate's centroid as a function of time in the absence of nocodazole treatment (top panel), after application of nocodazole (at the time point indicated with the solid arrow) to the rightmost 30% of the fragment with high level of MT self-nucleation (middle panel) or to the fragment with MT self-nucleation decreased to a low steady state level prior to nocodazole treatment (bottom panel); time points of a decrease in the level of MT self-nucleation and nocodazole treatment are indicated with dashed and solid arrows respectively.

Movie 1 Centering of the pigment aggregate in a nascent fragment (corresponds to stills shown on Fig. 1a).
Movie 2 Fluorescence speckle microscopy of microtubules in a nascent fragment (corresponds to stills shown on Fig. 1c).
Movie 3 Transport of pigment granules away from the cut edge along a MT nucleated on distal side (corresponds to stills shown on Fig. 2a).
Movie 4 Computational simulation of redistribution of the pigment aggregate in nascent fragment (corresponds to stills shown on Fig. 3a).
Movie 5 Aggreagtion of pigment granules in crescent-shaped fragment (corresponds to stills shown on Fig. 3b).

Suppelemental Methods.

Quantitative model of the centering mechanism.

General description of the model.

To confirm that the proposed mechanism can indeed drive the centering of the radial array in the absence of other centering mechanisms, we developed a two-dimensional computational model that simulates the centering kinetics. In the model, we simulate a melanophore fragment as a 40x10 m rectangle with 300 disks (d=0.5 m each) that mimic the pigment granules placed at the left margin of the rectangle to imitate the pigment aggregate in a nascent MT fragment. MTs in the simulations were depicted as lines that emerged (nucleated), elongated at one (plus) end, and shortened from the opposite (minus) end with rates described below.

Our model was based on the following *known* properties of pigment granules and MTs:
(1) *MTs are straight and immotile.* Live imaging of MTs indeed indicates that MTs do not bend significantly[1]; fluorescence speckle microscopy clearly showed that MTs in the fragments were always immotile (see Video 2).
(2) *MTs are nucleated on pigment granules and at random locations in the cytoplasm, with the majority nucleated on the granules.* Our past work described nucleation of MTs on pigment granules[2] and the present study indicates that MTs can also nucleate in the cytoplasm.
(3) *Nascent MTs grow in random directions at a constant rate of 4 m/min by elongation at the plus ends, which stabilize when they reach the cell cortex.* The rate of MT growth was taken from our past quantitative analysis of MT dynamics in melanophore fragments[1]. Stabilization of growing MT plus ends at the cortex was also documented in ref 11.
(4) *MTs shorten at the minus ends with constant rate that is equal to the rate of plus-end growth.* Measurement of the rates of plus-end growth and minus-end shortening indicated that they are balanced[1].
(5). *Pigment granules move to the minus ends of adjacent MTs with a constant velocity of 1 m/s.* We have recently performed detailed analysis of the movement of pigment granules along MTs in melanophores[3]. We found that while the granule movement in melanophores is discontinuous and involves occasional pauses and reversals, the average displacement toward the minus end occurred at approximately 0.8 m/s, which is close to the rate assumed in our current model.

We also *assumed* the following properties:
(6) *Minus ends of nascent MTs remain stable for about 60s.* In vivo, the random events of MT growth and shortening result in a wide range of MT lengths. For this study, we assumed that the average length of MTs in a fragment is approximately 4 m. To achieve this length, the plus ends of nucleated MTs should grow on average for 60s before the minus ends start shortening.

(7) *Frequency of MT nucleation in the fragments is 0.25 MT/min/ m^2.* Due to a high density of MTs, we found that it was impossible to measure MT nucleation frequency in the experiment. Based on a crude estimate of the total amount of MTs in the fragment (n=200), we assumed that the frequency of nucleation required to produce this number of MTs is approximately 0.25 MT/min/ m^2. This parameter was varied in our simulations and appeared to be non-critical to the outcome (see below).

(8) *Frequency of MT nucleation on granules is approximately10 times higher than spontaneously in the cytoplasm.* Based on our current and previously published observations, we found that the frequency of MT nucleation on granules is much higher than the frequency of spontaneous MT nucleation in the cytoplasm. We used the ratio of 10:1 in our initial simulations and varied this number to determine the likely ratio in vivo (see below).

(9) *Probability of spontaneous MT nucleation is equal at any area of the cytoplasm.* This assumption was supported by the results of our unpublished live microscopy observations, which indicated that MTs emerge at random locations in the cytoplasm.

The results of computational modeling based on the assumptions and experimental data are shown on Fig. 3 in the main text and Video 4. In close agreement with experimental results, the centering of the pigment aggregate in the simulations occurred within a half time of ten minutes. The distance from the centroid of the pigment aggregate and the center decreased exponentially, in agreement with the experiment (see below). Since under the experimental conditions the size and shape of the fragments can vary significantly, we ran simulations using rectangular fragments with the range of length and width between 20 and 70 m, which represent the lower and upper range of sizes for the experimentally produced fragments. We did not find correlation between the centering time and length or the ratio of length to width within the given range. To test this prediction, we measured the centering time in 12 fragments with lengths between 25 and 60 m and found that the correlation between the centering times and fragment lengths was indeed very low (see below). To test the accuracy of the model for fragments of different shape, we ran simulations with fragments of complex shapes (crescent, toroid, and oval) and compared the predicted location of the centered pigment aggregate in each type of fragment with those found under experimental conditions in similarly shaped fragments. Remarkably, the model was able to accurately predict the location of the centered pigment aggregate in the fragments of various shapes. For example, in crescent-shaped fragments the pigment aggregate always formed at the concave surface both in the simulations and in vivo in the microsurgically produced fragments. Similar correspondence between the model and experimental data was found for the fragments of other shapes (see below).

Thus, our model provides evidence that the spontaneous nucleation-dependent centering mechanism indeed follows from the in vivo parameters and accurately reflects the centering events observed in vivo. We also used the model to make additional observations and to test numerically the importance of various parameters that have served as the initial assumptions for the model. Based on these tests we made the following predictions:

(1) Observation of the centering kinetics in our simulations indicates that several cycles of MT disassembly and reassembly are required for the centering of the pigment aggregate. Therefore, plus-end MT growth rate is an important parameter that affects the centering time scale. We find that faster plus-end growth results in shorter times for the spontaneously nucleated MTs to reach the pigment aggregate, and therefore in the faster centering of the radial array. Slower plus-end growth results in the longer times and slower centering, respectively.

(2) The time of the delay in MT minus end destabilization is a critical parameter. By varying the delay time we find that longer delays lead to the slowing down the MT assembly and disassembly cycles and the centering, while shorter delays make the centering impossible, since the newly formed MTs cannot achieve the necessary length to 'feel' the fragment shape and establish a global directional bias. We found that the centering occurs normally if the delay time is in the range of 40 to 80s, which is consistent with the expected delay time in vivo.

(3) Changes in global rates of MT nucleation do not significantly affect the centering rate, but the ratio of MTs nucleated locally on the pigment granules to those nucleated at the random sites in the cytoplasm is of critical importance. In our simulations, if the fraction of spontaneously nucleated MTs was more than 25%, MT minus ends were no longer focused and the radial organization was lost. If the fraction of spontaneously nucleated MTs was less than 10%, the radial array was formed, but unable to move to the center of the fragment. Therefore in order for the radial array to form and relocate to the center, a delicate balance was essential between the rate of MT nucleation on the pigment granules and in the peripheral cytoplasm. Note that in our previous model[4] we considered the self-organization of the radial MT array dependent on granule-nucleated MTs. This model did not consider the self-nucleated MTs and could not explain centering in nascent fragments, so our present model significantly advances our understanding demonstrating that the self-nucleated MTs are crucial for the centering in addition (and in certain proportion to) MTs nucleated on granules, which are necessary for the radial MT array self-organization.

Mathematical analysis.

The following simple mathematical argument illustrates that the model of the centering suggested in this paper explains correctly the observed centering kinetics: let $x(t)$ be the pigment centroid position at time t (Fig. 3a, top). Then, one self-nucleated MT with its minus end at a distance y from the aggregate would move some granules away from the aggregate and shift its centroid by $x = sy$, where s is a dimensionless factor accounting for the probability of a MT passing through the aggregate and for the number of granules moved away from the aggregate by that MT (Fig. 3a, middle). The corresponding time interval, t, is defined by the MT growth with the rate V_{mt} : $\Delta t \sim y / V_{mt}$. The resulting effective rate of the aggregate shift is $v = \Delta x / \Delta t \sim s V_{mt}$. Multiplying this rate by the mean number of MTs self-nucleated in the cytoplasm, N_{cyt}, and averaging over the position of their minus ends, we obtain the mean centering velocity:

$$\langle v \rangle \approx sV_{mt} \times N_{cyt} \times \frac{1}{L} \times \left(\int_x^L dy - \int_0^x dy \right) = \frac{2sV_{mt}N_{cyt}}{L} \times \left(\frac{L}{2} - x \right).$$

Here L is the fragment's length. The solution of the differential equation, $dx/dt = \langle v \rangle$, has the form:

$$x = \frac{L}{2}\left(1 - e^{-t/T}\right), \quad T = \frac{L}{2sV_{mt}N_{cyt}}$$

and predicts that the pigment aggregate approaches the center with the rate slowing down exponentially, in full agreement with the observations (Fig. S1). In agreement with the experiment, the characteristic centering time T can be estimated as

$$T \ddot{y} \frac{40\mu m}{2 \cdot 0.025 \cdot 4\mu m/\min \cdot 20} \ddot{y} \, 10 \min \text{ for the fragment of characteristic length}$$

$L = 40\mu m$ assuming that there are $N_{cyt} \sim 20$ long self-nucleated MTs treadmilling with the rate $V_{mt} = 4\mu m/\min$. (We assume that the total MT number is $N_{tot} \sim 200$, and that $N_{cyt} = 0.1 N_{tot}$.) We estimate $s \sim (1/4) \cdot (N_{cyt}/N_{tot}) \sim 0.025$: the factor $(1/4)$ accounts for about 25% of MTs growing in the 'right' direction toward the granule aggregate, and we assume that the percentage of granules moved away from the aggregate is proportional to the ratio of the self-nucleated MT number to that of granule-nucleated MTs. Thus, the model predicts that if 10% of the long MTs are nucleated in the cytoplasm (the other 90% being nucleated on the granules), then the model successfully explains the time course of the centering. This simple calculation also predicts that the centering time does not depend on the fragment length. Indeed, assuming there is a constant nucleation rate per unit area of the cytoplasm, the number N_{cyt} is proportional to L, and time T is independent of L.

Computational model.

The model is implemented numerically as follows. We consider the movement of 300 composite pigment granules. At each moment, every granule is instantly transported to the minus end of any MT that passes within 0.4 m of the center of the granule. If there are several such MTs, one is chosen at random. Note that the time scale of granule movement (the corresponding characteristic time, $\sim 4\mu m/1\mu m/\sec = 4\sec$) is much faster than that of MT dynamics (minutes). The granules remain static if there are no MTs nearby. At each computational step, once all granules are transported to the respective minus ends, steric repulsion between granules is switched on such that granules repel each other strongly if their centers are closer to each other than a granule diameter (0.6 m in the simulations). This prevents the physical overlap of granules and models, realistically, the tight packing of the granules in the aggregate. The repulsion is switched off before the next cycle of granule movement allowing the granules to pass through each other during translocation to the minus ends.

MTs are nucleated at random in two manners, on granules and spontaneously in the cytoplasm, at average rates of one MT per granule per 5 minutes and 180 MTs per 5

minuntes, respectively. (This amounts to approximately $0.25/(\mu m^2 \times sec)$ net nucleation rate.) Their orientations are random and their appearance is exponentially distributed in time. MT minus-ends that are uninfluenced by granules switch from the immobile to shrinking state at a rate of 1/min. When granules are close enough to minus-ends to influence their dynamics (0.4 m), they switch from the immobile to shrinking state at a rate of 0.2/min and from shrinking to immobile at a rate of 1.4/min.

The plus ends grow at a constant rate and stall when they reach the fragment edges. This stability of the plus ends at the boundary is important: if the plus end catastrophes upon reaching the boundary, simulations show that MTs do not establish a global directional bias. Shrinking minus ends move at the same constant rate as the plus ends. A MT disappears when the depolymerizing minus end reaches the plus end stalled at the edge.

For simulations, we nondimensionalize the model using the characteristic fragment size, 40 m, as the unit of length, and the ratio of the fragment size to the MT treadmilling rate, (40 m)/(4 m/min) = 10 min, as the unit of time. The simulation time step is equal to 0.02 of the unit of time = 12 sec of real time. The numerical code was written using Matlab™ and the simulations were performed on a desktop computer.

Robustness of the model and effect of the nucleation rates.

Qualitatively, the model is robust with respect to changes of the rates within a few fold, provided the total number of the long self-nucleated MTs is between 5% and 25% of the total average MT number. Too few self-nucleated MTs do not support centering at all; too many disrupt pigment aggregation. The nucleation rates we used are such that the ratio of the number of MTs longer than 4 m that were nucleated in the cytoplasm to the number nucleated on granules is close to 10%, and the total MT number is ~ 200. In the simulations, self-nucleated MTs are shorter on average than MTs nucleated on the granules: the ratio of the total number of self-nucleated MTs to the number nucleated on granules is close to 30%, while the ratio of the number of self-nucleated MTs longer than 10 m to the number nucleated on granules is close to 3-5%.

Figure S1 shows the simulation results confirming the analytical predictions in the main text that the centering time stays almost constant as the total nucleation rate varies a few folds with the ratio of the MT nucleated on granules and in the cytoplasm held constant. When this ratio varies, with the total nucleation rate held constant, the centering time is inversely proportional to the number of the self-nucleated MTs. Note that the centering time reaches a minimum, approximately equal to 20 min, when the ratio of the number of MTs longer than 4 m that are nucleated in the cytoplasm to the number nucleated on granules is close to 10%. Further increase of the self-nucleation rate is not effective.

The pigment granules aggregate to the fragment's centroid.

The simulations demonstrate that in fragments of various shapes the pigment granules aggregate within a few tens of minutes to the centroids of the respective fragments (Fig.

S3). Intuitively, this is easy to understand: the aggregate is located so that *on average* its centroid is not displaced by self-nucleated MTs with minus ends distributed uniformly throughout the fragment, which mathematically means $\sum_{i \subset \Omega} \vec{y}_i = 0$, where $\vec{y}_i$ is the vector between the minus end of the ith self-nucleated MT passing through the granules and the aggregate, and Ω is the fragment's area. The formula $\sum_{i \subset \Omega} \vec{y}_i = 0$ is precisely the definition of the centroid of the fragment.

Fragment size and centering time are not correlated.

We experimentally looked for a correlation between the fragment size and centering time by measuring the centering kinetics in 12 fragments of similar width and lengths varying from 25 to 70 m. The centering time varied considerably, from a few to almost 2000 sec. The data is plotted in Fig. S2. The mean measured centering time is 756 sec, and its standard deviation is 580 sec. The mean distance traveled by the centroid of the aggregate is equal to 20.1 m and its deviation is 6.4 m. We used Matlab™ to calculate the linear correlation between the distance and centering time (using the function *corrcoef*). The corresponding correlation coefficient is approximately 0.3 meaning a very low degree of correlation between the fragment size and centering time, in agreement with the model prediction.

Modeling local application of nocodazole.

We mimicked the experiment with local application of nocodazole by lowering the MT nucleation rate to zero in the area from 0.7 to 1 of the fragment length. The simulation demonstrated that in that case the granules center to the middle of the nocodazole-free area of the fragment (Fig S4, middle). We checked that the re-centering does not takes place if the nucleation rate is lowered near one of the fragment's edges after the centering is completed, when the MT nucleation rate in the cytoplasm decreases (Fig. S4, bottom). Note that the stochastic variance of the pigment's centroid is very large in the process of the centering and then decreases after the centering completion (Fig. 3a). This is consistent with the model: the variance in the position of the fragment is driven by the stochastic arrival of anti-astral MTs at the aggregate, a process that is more prevalent during the transient period of elevated MT nucleation that occurs during the nucleation-dependent centering. Thus, the model confirms that asymmetric MT nucleation and treadmilling can indeed account for the complex events that occur during the centering of a MT array.

Centering kinetics.

The simulations (Video 4) showed that the centering time scale is determined simply by the time needed to turn over the MTs a few times. The centroid of the granule aggregate approached the center of the fragment exponentially (Fig S4, top).

Spontaneous MT nucleation increases robustness of centrosomal centering.

In ref. 12 we demonstrated that on the average, a local vector sum of movements or forces causing movements in the cytoplasm can be effectively treated mathematically as a linear combination of advection and diffusion. The corresponding advection and diffusion rates, $\vec{V}(\vec{x})$ and $D(\vec{x})$, respectively, are local functions of the coordinate, $\vec{x}$. In the simplest case, in the discoid fragment of radius R, the functions $\vec{V}(r)$ and $D(r)$ are radially symmetric (r is the distance from the center of the fragment). Let us assume that a dominant, force-dependent, mechanism of centrosomal centering is characterized in such simple case by the effective advection $\vec{V}_f(r)$ and diffusion $D_f(r)$. The spontaneously nucleated MTs would establish an additional bias toward the center, because if we assume the presence of dynein motors on the centrosome, these motors would transport the centrosome toward the minus ends of the spontaneously nucleated MTs. This spontaneous nucleation centering mechanism would be characterized by the effective advection $\vec{V}_s(r)$ and diffusion $D_s(r)$. It was shown in ref[4] and by Maly and Borisy[5] that $\vec{V}_s(r) \sim r/R, D_s(r) \sim (R-r)^2/R^2$. The magnitude of the force-dependent centering mechanism is likely to be much stronger, than that of the spontaneous nucleation mechanism, because tens of molecular motors are responsible for the former, while few motors can move centrosome along a single MT, so $\vec{V}_s(r) \quad \vec{V}_f(r), D_s(r) \quad D_f(r)$. The velocities of the combined mechanism add: $\vec{V}_{comb} = \vec{V}_f(r) + \vec{V}_s(r)$, while the combined diffusion coefficient is $D_{comb} = \sqrt{\left[D_f(r)\right]^2 + \left[D_s(r)\right]^2}$ (ref.[6]).

Let us introduce the probability distribution $p(\vec{x})$ for the centrosome to be located at $\vec{x}$. In the equilibrium, this probability distribution can be found from the condition that the total advection and diffusion flux is equal to zero: $\vec{V}_{comb}(\vec{x})p(\vec{x}) - D(\vec{x})\nabla p(\vec{x}) = 0$

(ref.[6]). In the radially symmetric case, $(V_f(r) + V_s(r))p(r) + D_{comb}(r)\dfrac{dp}{dr} = 0$, where the velocities are positive toward the center of the fragment. The resulting probability distribution is $p(r) = p(0) \times \exp\left[-\int_0^r \dfrac{V_f(s) + V_s(s)}{D_{comb}(s)} ds\right]$. Using strong inequalities

$\vec{V}_s(r) \quad \vec{V}_f(r), D_s(r) \quad D_f(r)$, and neglecting small terms of order $\left(D_s/D_f\right)^2$, this probability distribution can be re-written in the form:

$$p(r) \approx p(0) \times \exp\left[-\int_0^r \frac{V_f(s)}{D_f(s)} ds\right] \times \exp\left[-\int_0^r \frac{V_s(s)}{D_f(s)} ds\right].$$

Without the spontaneous nucleation mechanism, $p(r) = p(0) \times \exp\left[-\int_0^r \dfrac{V_f(s)}{D_f(s)} ds\right]$, so the redundant spontaneous nucleation centering mechanism increases the probability of proper centering. Simple asymptotic analysis demonstrates that the redundant spontaneous nucleation centering mechanism increases the probability of centering by the

$$\text{factor} \sim 1 + 2\left[\left(\int_0^r V_s(s)\,ds\right)\left(\int_0^r V_f(s)\,ds\right)\right].$$ Thus, if the spontaneous nucleation centering

mechanism is 5-10% as strong, as the dominant force-dependent mechanism, then the weak redundant mechanism still increases the probability of centering by 10-20%.

Chemical gradient cannot explain centering in fragments of certain shapes.

One possible mechanism of centering could be chemically regulated heterogeneity of MT kinetics. For example, if either MT nucleation or treadmilling rates depend on the concentration of an activated kinase, and if such a kinase is activated on the fragment boundaries and de-activated spontaneously in the cytoplasm, then a stable activated kinase gradient can be established in the fragment[7]. The corresponding concentration would be highest on the boundary and lowest in some internal location(s). If the lowest kinase concentration induces a maximal nucleation rate and/or a minimal minus end shrinking rate, then the MT aster can form with its focal point at a local minimum of the kinase concentration. However, first, we did not notice significant differences in the MT kinetic rates in different locations inside the fragment. Second, from a theoretical point of view, if the kinase is activated uniformly along the fragment boundary, then the local concentration minimum coincides with the fragment centroid in the simple symmetric fragments having circular, ellipsoidal and rectangular shape. In crescent-shape fragments, calculations (not shown) demonstrate that the local minimum of the kinase concentration does not coincide with the fragment's centroid, but the distance between the minimum and the centroid is too small to be noticed experimentally. Thus, fragments of these shapes do not allow rejecting the chemical gradient hypothesis. Fortunately, there is a fragment shape which unequivocally demonstrates that the chemical gradient would fail to explain centering phenomenon: in ref. 12 we demonstrated experimentally and theoretically that the MT asters in the bi-lobed fragments consisting of two lobes connected with a narrow 'corridor' migrates to the center of the corridor. If the kinase was activated along the boundary in the fragment of this shape, then there would be two local concentration minima in the centers of the respective lobes, because the narrow corridor boundaries would not contribute significantly to the kinase distribtution. There would be also a high kinase concentration inside the corridor, so the chemical regulation mechanism would predict a stable self-organization of two MT asters centered in their respective lobes. The experiment, however, showed merging of two such asters in the center of the corridor, challenging the hypothetical chemical regulation mechanism.

References.

1. Rodionov, V.I. & Borisy, G.G. Microtubule treadmilling in vivo. *Science* **275**, 215-8 (1997).
2. Vorobjev, I., Malikov, V. & Rodionov, V. Self-organization of a radial microtubule array by dynein-dependent nucleation of microtubules. *Proc Natl Acad Sci U S A* **98**, 10160-5 (2001).
3. Zaliapin, I., Semenova, I., Kashina, A. & Rodionov, V. Multiscale trend analysis of microtubule transport in melanophores. *Biophys J* **88**, 4008-16 (2005).

4. Cytrynbaum, E.N., Rodionov, V. & Mogilner, A. Computational model of dynein-dependent self-organization of microtubule asters. *J Cell Sci* **117**, 1381-97 (2004).

5. Maly, I.V. & Borisy, G.G. Self-organization of treadmilling microtubules into a polar array. *Trends Cell Biol* **12**, 462-5 (2002).

6. Berg, H. Random walks in cell biology. Princeton: Princeton University Press (1983).

7. Wollman, R. et al. Efficient chromosome capture requires a bias in the 'search-and-capture' process during mitotic-spindle assembly. *Curr Biol* **15**, 828-32 (2005).